STUDY OF DUAL DIFFRACTIVE MODELS IN PROCESS $pp \to pn\,\pi^+$ AT 12 GeV/c

BY V. KUNDRÁT* AND M. ZRAŁEK

Institute of Physics, Jagellonian University, Cracow**

(Received February 15, 1973)

The Pokorski-Satz and the Dorren-Rittenberg-Yaffe models for diffractive process $pp \to pn\,\pi^+$ at 12 GeV/c are tested. The Dorren-Rittenberg-Yaffe model is tested with 0.0, 0.3, and 0.5 pomeron slopes. This model has only two free parameters (the overall normalization constant and relative coupling constant) and gives a reasonably good agreement with the data for the pomeron slope of 0.3 and 0.5. In particular, it gives the correct angular distributions in the Gottfried-Jackson angle on the $n\pi^+$ system. The distribution in azimuthal angle $\Phi(n\pi^+)$ in Gottfried-Jackson and helicity frames are not flat which means that helicity is not conserved both neither in t- nor in s-channels. The Pokorski-Satz model also reasonably describes the data except for the angular distributions in the Gottfried-Jackson frame.

1. Introduction

After a successful application of dual models to the non-diffractive processes [1–3] an attempt of incorporating the pomeron exchange into the dual framework has been made by Pokorski and Satz [4] and by Satz and Schilling [5]. In the diffraction dissociation vertex (*cf.*, Fig. 1a) one observes in general both direct and crossed channel exchange effects [4], therefore the dual description of the upper vertex (Fig. 1a) seems to be very natural. The Pokorski and Satz (PS) model has, however, serious difficulties with the high energy double Regge limit. These difficulties became a starting point for Dorren, Rittenberg and Yaffe [6] who constructed another model of diffractive dissociation with a correct double Regge high energy behaviour.

The aim of this paper is to compare the predictions of the two models for the invariant mass, momentum transfer and angular distributions with the experimental data from Bonn–Hamburg–Munich Collaboration for the diffractive process $pp \to pn\,\pi^+$ at 12 GeV. The angular distributions are emphasized as they offer a sensitive test of production dynamics.

---

* On leave of absence from Institute of Physics of ČSAV, Prague (present address). Supported by the UNESCO Copernicus fellowship.

** Address: Instytut Fizyki, Uniwersytet Jagielloński, Reymonta 4, 30-059 Kraków, Poland.

In Chapter 2 we briefly discuss the two models, stressing the differences between them. In particular the Dorren, Rittenberg and Yaffe (DRY) model describes better the angular distributions in the Gottfried-Jackson frame of the $n\pi^+$ system than the PS model. We also find that the double Regge limit of the single Regge limit of the B_5 function is identical with the double Regge limit of the same B_5 function, in contrast to the results of Ref. [6].

Chapter 3 contains theoretical predictions of the two models for the $M(n\pi^+)$ and $M(p\pi^+)$ effective mass distributions, for the distributions of momentum transfer between the target and recoil protons and of momentum transfer between the beam proton and neutron.

The gross features of these distributions are reproduced by both models. Chapter 3 contains farther the discussion of angular distributions in cosine of the Gottfried-Jackson angle $\cos \Theta_{GJ}$ of the $n\pi^+$ system. In particular these angular distributions give in the DRY model a backward enhancement which is absent in the PS model.

The angular distributions in the azimuthal angle $\Phi(n\pi^+)$ in the Gottfried-Jackson and helicity frames are strongly influenced by the kinematical cut in s_{3B}. In the DRY model the angular distributions are not flat, even without the kinematical cut. This means that helicity is not conserved neither in the s-channel nor in t-channel. In the PS model the distribution in the $\Phi_{TY}(n\pi^+)$ is determined only by phase-space and is flat without the cut in s_{3B}. The cut in s_{3B} improves the agreement with the data around $\Phi = 0$ but the disagreement around $\Phi = \pm\pi$ still remains.

To summarize, the DRY model gives distributions which reproduce the data quite well if the pomeron slope is not zero.

2. Description of Pokorski-Satz and Dorren-Rittenberg-Yaffe models

The Pokorski-Satz model is based on an assumption of the factorization of the amplitude into the lower vertex function $e^{1/2\, at_1}$ taken from the asymptotic elastic scattering and the upper vertex function V describing the process $1+\mathbf{p} \to 2+3$ (our kinematics explained in Fig. 1). Assuming the pomeron trajectory of zero slope and unit intercept, Pokorski and Satz postulate the following form of the amplitude

$$M \sim e^{1/2at_1} s_{1A} V. \tag{2.1}$$

To incorporate the incident nucleon spin, they decompose the upper vertex function V into the invariant spin amplitudes $A(\alpha_{12}, \alpha_{23}, \alpha_{13})$ and $B(\alpha_{12}, \alpha_{23}, \alpha_{13})$, each of them being the symmetrized four-body Veneziano amplitude

$$B_4(-\alpha_{23}, -\alpha_{12}) + B_4(-\alpha_{23}, -\alpha_{13}) + B_4(-\alpha_{12}, -\alpha_{13}). \tag{2.2}$$

Here B_4 is the Euler beta function and α_{ij} the Regge trajectory in $\{i, j\}$ channel. The spins of target and recoil nucleons A and B are ignored in the model.

It is obvious that the amplitude (2.1) has a correct high energy Regge behaviour in s_{1A}. Dorren *et al.* [6] noticed that the double Regge limit of amplitude (2.1) does not coincide with its usual form. This is caused by the fact that the pomeron propagator

($s_{1A}^{\alpha_P} = s_{1A}$) in Eq. (2.1) depends only on s_{1A} and not on s_{3B}. Similar comments are also made in Refs [7, 8] where the factor s_{1A} is substituted by other effective factors.

On the other hand the Bardakçi-Ruegg-Virasoro [9] function has the correct single and double Regge limits [9, 10]. The idea of Dorren, Rittenberg and Yaffe was to write down the single Regge limit of B_5 function, which factorizes in this limit into a product of terms describing the upper and lower vertices. Using the pomeron trajectory with arbitrary

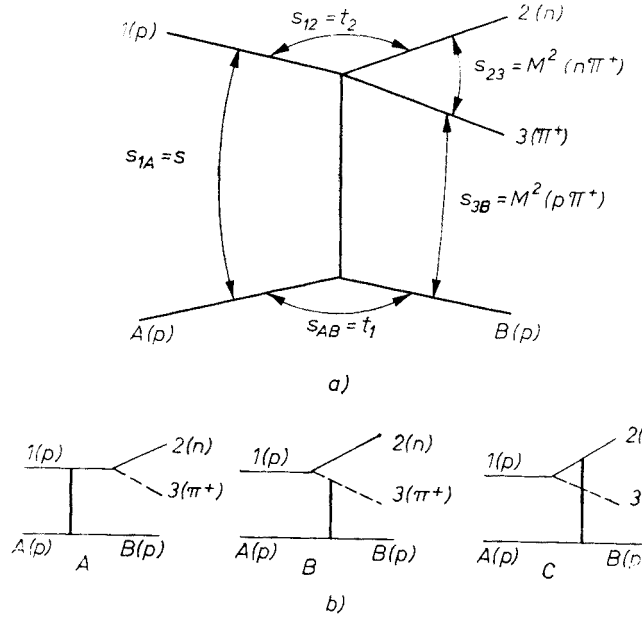

Fig. 1. a) Kinematics of the process $pp \to pn\pi^+$. b) Graphs of the Ross and Yam model for the processes $pp \to pn\pi^+$

slope, adding the lower vertex function (taken from asymptotic high energy scattering) and symmetrizing the amplitude, Dorren *et al.* finally obtain the following expression

$$M \sim e^{1/2at_1}\Gamma(1-\alpha_p)\left(\frac{s_{1A}}{s_0}\right)^{\alpha_p}(1+e^{-i\pi\alpha_p})\times$$

$$\times \int_0^1 dx[x^{-\alpha_{23}-1}(1-x)^{-\alpha_{12}-1}|1-(1-K)x|^{\alpha_p}+$$

$$+x^{-\alpha_{23}-1}(1-x)^{-\alpha_{13}-1}|1-Kx|^{\alpha_p}+x^{-\alpha_{13}-1}(1-x)^{-\alpha_{12}-1}|K-1+x|^{\alpha_p}]. \qquad (2.3)$$

Here $s_0 = 1$ GeV^2, α_p is the pomeron trajectory and $K = \alpha_{3B}/\alpha_{1A}$ is kept fixed. This form of amplitude is assumed to be valid for high energies s_{1A}.

The double Regge limit of B_5 function [10, 11] is obtained in the limit s_{3B}, s_{23}, $s_{1A} \to \infty$, keeping $\xi = \alpha_{3B}\alpha_{23}/\alpha_{1A}$ fixed. The amplitude M in Eq. (2.3) reduces to the same expression as in Ref. [9] if $s_{23} \to \infty$ (for details see Appendix 1). In this point we disagree with Ref. [6].

Comparing Eqs (2.1) and (2.2) with Eq. (2.3) one sees that both amplitudes are identical if the terms with absolute values in Eq. (2.3) are equal to one. However, all these factors cannot be equal to unity at the same time. Therefore the PS model cannot be considered as a special case of the DRY model. For instance the additional terms (those with absolute values in Eq. (2.3)) change the residues of the daughters [10].

The difference of the two models can be illustrated *e.g.* in the angular distribution in the Gottfried-Jackson angle Θ_{GJ} of the $\{2, 3\}$ system. The diffractive process $1+A \to 2+3+B$ can be reproduced by the sum of the graphs (double diffractive dissociation diagram is neglected) which are shown in Fig. 1b. The contributions of individual graphs A, B, and C to the total amplitude are proportional to

$$\frac{E_1^{\mathrm{LAB}}}{m_1^2 - s_{23}}, \quad \frac{E_3^{\mathrm{LAB}}}{m_3^2 - s_{12}} \text{ and } \frac{E_2^{\mathrm{LAB}}}{m_2^2 - s_{13}} \tag{2.4}$$

respectively [12]. These terms are identical in the high energy limit [13–14].

In the process $pp \to pn\pi^+$ we have $m_3^2 = m_\pi^2 \approx 0$ and the denominator in the second term of Eq. (2.4) strongly depends on the cosine of Θ_{GJ} in the rest frame of $n\pi^+$ system. As the first term in Eq. (2.4) does not depend on $\cos\Theta_{GJ}$, the lab energy E_3^{LAB} must compensate this dependence on $\cos\Theta_{GJ}$ of the denominator in the second term of Eq. (2.4).

In the PS model all energies in the nominators are identical ($s_{1A} \sim E_1^{\mathrm{LAB}}$) and do not depend on $\cos\Theta_{GJ}$. This means that the strong dependence of denominator on $\cos\Theta_{GJ}$ in the second term is not compensated. Therefore we expect the PS model to give the angular distribution in $\cos\Theta_{GJ}$ strongly peaked in the very forward direction as $s_{12} \sim 0$ for $\cos\Theta_{GJ} \sim 1$.

On the other hand, the DRY model gives the correct form of all terms in Eq. (2.4) and we expect an improvement in the angular distributions in $\cos\Theta_{GJ}$ [15].

The above considerations are valid only for an amplitude with a flat pomeron and in the high energy limit, but we expect that the difference in angular distributions as predicted by the two models will be visible even at finite energies.

3. Application of the models to the process $pp \to pn\pi^+$ *at 12 GeV/c*

For both $\{2, 3\}$ and $\{1, 3\}$ channels we consider only the non-degenerate baryon trajectories N_α and N_γ in the form

$$\begin{aligned} \alpha_{N_\alpha} &= -0.4 + s + i0.16(s-\bar{s})\theta(s-\bar{s}), \\ \alpha_{N_\gamma} &= -0.8 + s + i0.16(s-\bar{s})\theta(s-\bar{s}), \end{aligned} \tag{3.1}$$

where $\bar{s}$ denotes the πN effective mass threshold.

In the $\{1, 2\}$ channel the π and the A_1 trajectories can be exchanged. Since the A_1 trajectory is much weaker coupled to the $N\bar{N}$ vertex than the π trajectory, we suppose that only the π trajectory

$$\alpha_\pi = -0.02 + s \tag{3.2}$$

can be exchanged in this channel. This simplifies the amplitudes in both models. Thus the contribution from the B invariant amplitude in the PS model can be neglected [4]. As we are not interested in polarization effects, we must sum over all final nucleon spin states and average over all initial nucleon spin states. This adds the additional factors of $|s_{12}|$ to the absolute square of PS amplitude (2.1). This way of including spins in the upper vertex cannot be applied in DRY model and the factor $|s_{12}|$ in their amplitude is introduced phenomenologically.

Taking into account only the exchange of two trajectories (3.1) the absolute square of the PS amplitude can be written as

$$|M|^2 = ce^{at_1} s_{1A}^2 |V^+ + \lambda V^-| \, |s_{12}| \, . \tag{3.3}$$

Here c is a normalization constant and λ the relative coupling of both amplitudes

$$V^\pm = B_4(\tfrac{1}{2} - \alpha_{23}, -\alpha_{12}) \pm B_4(\tfrac{1}{2} - \alpha_{23}, \tfrac{1}{2} - \alpha_{13}) + B_4(\tfrac{1}{2} - \alpha_{13}, -\alpha_{12}). \tag{3.4}$$

The $+$ $(-)$ sign corresponds to the $N_\alpha(N_\gamma)$ trajectory and the $\frac{1}{2}$ is added to obtain the baryon resonances at the right places. Similarly under the same assumptions the absolute square of DRY amplitude can be written as

$$|M|^2 = ce^{at_1} |s_{12}| \left| \frac{1 - e^{-i\pi\alpha' t_1}}{\alpha' t_1} \Gamma(1 - \alpha' t_1) \left(\frac{s_{1A}}{s_0} \right)^{\alpha_p} \right|^2 |V^+ + \lambda V^-|^2. \tag{3.5}$$

Here α' means the pomeron slope, c the normalization constant and λ the relative coupling of amplitudes corresponding to N_α and N_γ exchange. With the help of the hypergeometric functions ${}_2F_1$ [16], the following expressions for $V^+(V^-)$ can be obtained from Eq. (2.3)

$$\begin{aligned} V^\pm = {} & B_4(\tfrac{1}{2} - \alpha_{23}, -\alpha_{12}) {}_2F_1(\tfrac{1}{2} - \alpha_{23}, -\alpha_p; \tfrac{1}{2} - \alpha_{23} - \alpha_{12}; 1 - K) \pm \\ & \pm B_4(\tfrac{1}{2} - \alpha_{23}, \tfrac{1}{2} - \alpha_{13}) {}_2F_1(\tfrac{1}{2} - \alpha_{23}, -\alpha_p; 1 - \alpha_{23} - \alpha_{13}; K) + \\ & + (1 - K)^{1/2 - \alpha_{13} + \alpha_p} B_4(\tfrac{1}{2} - \alpha_{13}, 1 + \alpha_p) {}_2F_1(1 + \alpha_{12}, \tfrac{1}{2} - \alpha_{13}; \tfrac{3}{2} - \alpha_{13} + \alpha_p; 1 - K) + \\ & + K^{-\alpha_{12} + \alpha_p} B_4(-\alpha_{12}, 1 + \alpha_p) {}_2F_1(-\alpha_{12}, \tfrac{3}{2} + \alpha_{13}; 1 - \alpha_{12} + \alpha_p; K). \end{aligned} \tag{3.6}$$

This form of amplitude is similar to that proposed in Ref. [17] and can be essentially simplified for a flat pomeron. The expressions (3.3)–(3.6) have been used in numerical calculations with a fixed parameter $a = 10\ \mathrm{GeV}^{-2}$ characterizing the slope of the diffraction peak.

The models are tested using the data from Ref. [18] for the process $pp \to pn\pi^+$ at 12 GeV/c, where the following kinematical cuts have been made

$$0.02 < |t_1| < 1.0\ \mathrm{GeV}^2, \ s_{3B} > 4\ \mathrm{GeV}^2, \ t_2 > -0.8\ \mathrm{GeV}^2. \tag{3.7}$$

We use the same kinematical cuts in our calculations and use the same Regge trajectories for both models. All graphs are normalized to the same number of events as in experiment.

The calculations have been performed using the Monte Carlo program FOWL [19] and checked in a few points by direct integration.

There are only two free parameters in our formulation of the problem: the overall normalization constant c and the relative coupling constant λ of the baryon trajectories N_α and N_γ. These parameters are fitted from the $M(n\pi^+)$ effective mass and cos Θ_{GJ} angular distributions in the mass interval (1.1–1.7) GeV at fixed value α' of pomeron slope. In

TABLE I

Fitted values of the relative coupling constant λ in the two models at fixed values of pomeron slope α'

Model	α'	λ
PS	0.0	1.770
DRY	0.0	0.079
DRY	0.3	0.065
DRY	0.5	0.055

Table I are shown all fitted values of the relative coupling constant λ. The relatively small values of λ in DRY amplitude are due to the fact that the term N_γ in the amplitude (3.5) is of one order of magnitude greater than the N_α term.

3a. The $M(n\pi^+)$ effective mass distribution

The effective mass distribution of the neutron and the meson is shown in Fig. 2. Its shape is determined by the trajectory in the diffractive channel {2, 3}, by the pomeron slope and is influenced by kinematical cuts in s_{3B} and t_2.

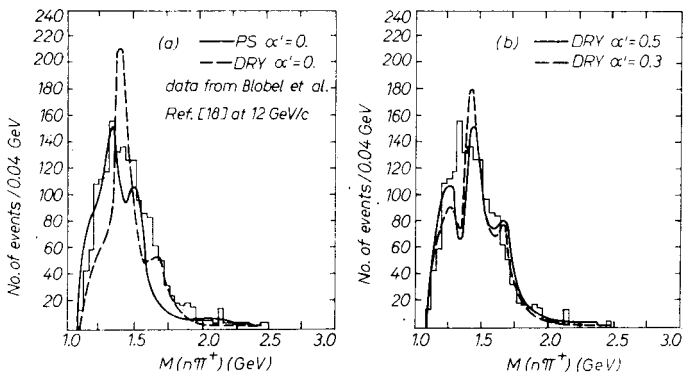

Fig. 2. $M(n\pi^+)$ effective mass distribution of the $n\pi^+$ system In Fig. a the solid (dashed) curve corresponds to the PS (DRY) model with a flat pomeron while in Fig. b the solid (dashed) curve represents the DRY model predictions for 0.5 (0.3) pomeron slope

In the PS model (*cf.* Fig. 2a) the curve shows two peaks corresponding to the main contributions from the N_α and N_γ trajectories. The peak at 1340 MeV is given by the first daughter of the N_α trajectory at $J = 3/2$ and by the Deck-type effect and the peak at 1500 MeV is caused by the $J = 3/2$ pole from the N_γ trajectory. The dip at 1420 MeV is caused by a destructive interference between N_α and N_γ amplitudes.

On the contrary, the DRY model predictions show a constructive interference between both amplitudes resulting in a single peak at $\sim$ 1400 MeV which decreases and moves to the higher mass values of $M(n\pi^+)$ with increasing pomeron slope. Small peaks in all DRY model predictions at 1680 MeV correspond to the first Regge recurrence of N_α trajectory and their values increase with pomeron slope.

An increasing peak at 1260 MeV has its origin in the background terms of diffractive {2, 3} channel of (3.5) amplitude (similar to the Deck effect). This is not significant in the case of a flat pomeron and arises only at higher values of pomeron slope. It is seen that neither the PS nor the DRY models reproduce the $M(n\pi^+)$ effective mass distribution well enough due to dips in the Roper region.

3b. $M(p\pi^+)$ effective mass distribution

The $M(p\pi^+)$ effective mass distribution of the recoil proton and the π meson is shown in Fig. 3. It is strongly influenced by the kinematical cut in $s_{3B} = M^2(p\pi^+) > 4$. As the PS amplitude in Eqs (3.3)–(3.4) does not depend on s_{3B}, the $M(p\pi^+)$ distribution is determined in this model by phase-space. The DRY model predictions agree better with the data than the predictions of the PS model. Lower $M(p\pi^+)$ values may be enhanced by increasing the pomeron slope. The best fit corresponds to the pomeron slope of 0.5.

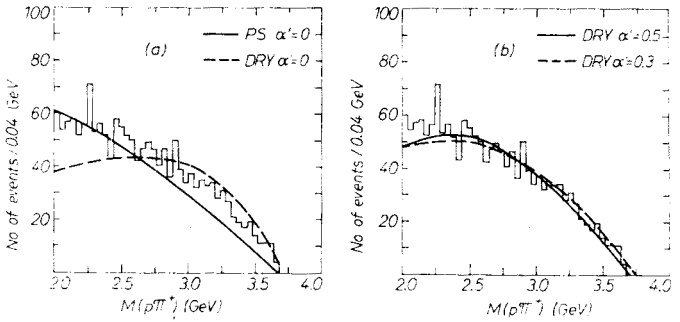

Fig. 3. $M(p\pi^+)$ effective mass distribution of the $p\pi^+$ system

3c. Momentum transfer t_1 distribution between target and recoil protons

Fig. 4 shows the momentum transfer t_1 distribution between the target and the recoil protons. The curve corresponding to the PS model is too steep and does not reproduce the data well enough. The same holds for the DRY curve corresponding to the value of pomeron slope 0.5. Generally, the higher is the pomeron slope, the steeper is the momentum transfer distribution in t_1. These results may be adjusted by a slight change of the parameter a characterizing the diffraction peak. Its value was kept fixed throughout our calculations.

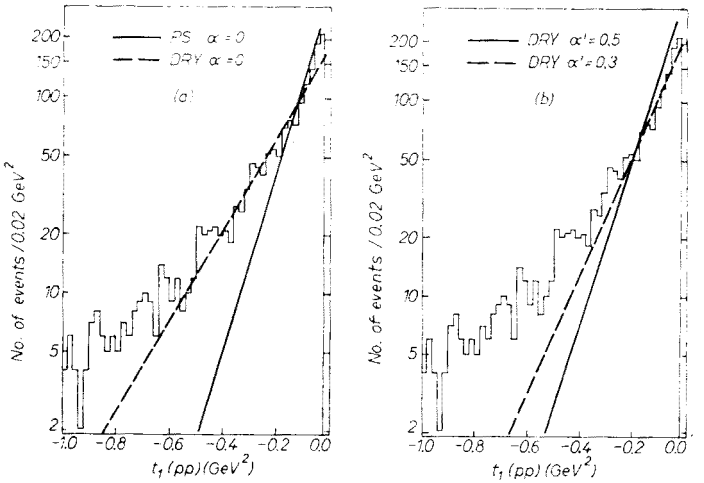

Fig. 4. Distribution of momentum transfer t_1 from the target proton to the recoil proton

3d. Momentum transfer t_2 distribution between beam proton and neutron

The momentum transfer t_2 distribution between the beam proton and neutron is presented in Fig. 5. All curves feature an enhancement at small values of $|t_2|$. The PS model deviates from the data at higher $|t_2|$ values. The DRY model for the flatpomeron also deviates from the data but at small $|t_2|$ values. However increasing the pomeron slope impro ves the agreement with data. This indicates that in this model we should perform our calculations with a non-flat pomeron. With increasing pomeron slope the peak at small $|t_2|$ values of momentum transfer t_2 distribution increases and the enhancement at higher $|t_2|$ values is depressed.

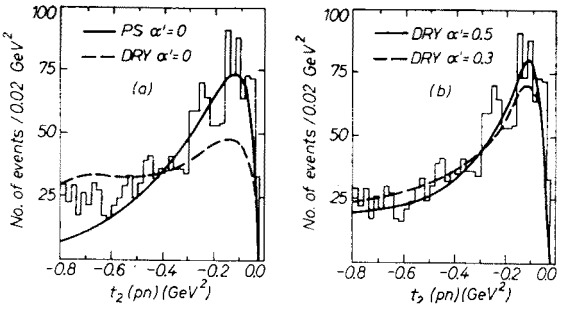

Fig. 5. Distribution of momentum transfer t_2 from the beam proton to the neutron

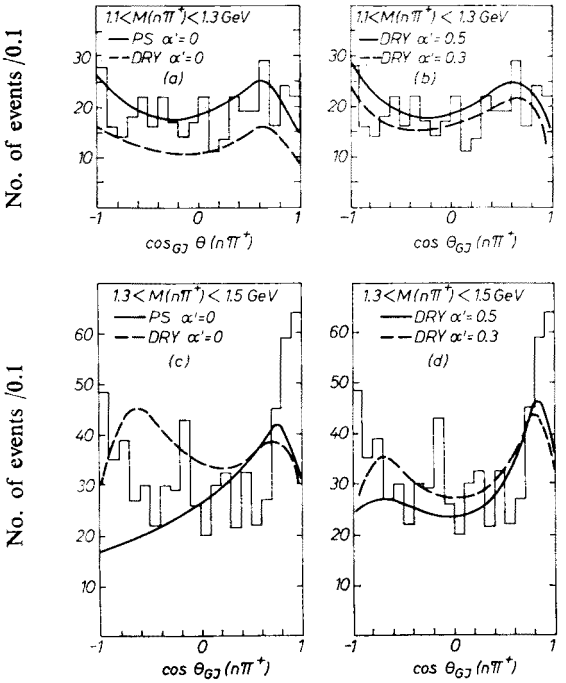

Fig. 6. Angular distribution of the cosine of the Gottfried-Jackson angle cos $\Theta_{GJ}(n\pi^+)$ for $1.1 < M(n\pi^+) < 1.3$ GeV and $1.3 < M(n\pi^+) < 1.5$ GeV; a) solid (dashed) curve corresponds to the PS (DRY) model for a flat pomeron for $1.1 < M(n\pi^+) < 1.3$ GeV; b) solid (dashed) curve corresponds to the DRY model predictions with 0.5 (0.3) pomeron slope for $1.1 < M(n\pi^+) < 1.3$ GeV; c) solid (dashed) curve corresponds to the PS (DRY) model for a flat pomeron for $1.3 < M(n\pi^+) < 1.5$ GeV; d) solid (dashed) curve corresponds to the DRY model predictions with 0.5 (0.3) pomeron slope for $1.3 < M(n\pi^+) < 1.5$ GeV

3e. Distribution of the Gottfried-Jackson angle Θ_{GJ} of the $n\pi^+$ system

The angular distribution of the cosine of the Gottfried-Jackson angle between beam proton and neutron in the $n\pi^+$ system provides a sensitive test of production dynamics. The results from both models are shown in Figs 6 and 7 for various effective $M(n\pi^+)$ mass intervals. They depend strongly on the intercept of the trajectory in the diffractive {2, 3} channel and on the kinematical cuts. Generally, the PS model gives a peak in the very forward direction without any significant enhancement in backward direction. The DRY model on the contrary gives this backward enhancements in agreement with the data. The value of this backward enhancement is influenced by the used kinematical cuts. The PS model predictions indicate only a peak in the forward direction and this peaking does not depend on the kinematical cuts (mainly the cut in t_2). This disagrees with the unpublished Scandinavian data at 19 GeV/c [20], where no kinematical

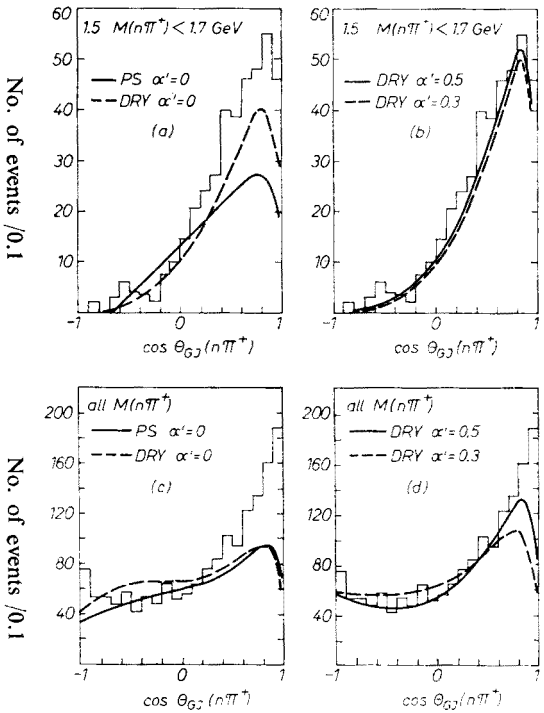

Fig. 7. Angular distribution of the cosine of the Gottfried-Jackson angle cos Θ_{GJ}(n,π^+) for 1.5 < $M(n\pi^+)$ < 1.7 GeV and 1.1 < $M(n\pi^+)$ < 1.7 GeV; a) solid (dashed) curve corresponds to the PS (DRY) model for a flat pomeron for 1.5 < $M(n\pi^+)$ < 1.7 GeV; b) solid (dashed) curve corresponds to the DRY model predictions with 0.5 (0.3) pomeron slope for 1.5 < $M(n\pi^+)$ < 1.7 GeV; c) solid (dashed) curve corresponds to the PS (DRY) model for a flat pomeron for 1.1 < $M(n\pi^+)$ < 1.7 GeV; d) solid (dashed) curve corresponds to the DRY model predictions with 0.5 (0.3) pomeron slope for 1.1 < $M(n\pi^+)$ < 1.7 GeV

cut in t_2 is made. The dips in the very forward direction in all distributions are caused by the kinematical cut in s_{3B}, while the very backward dips are due to the cut in t_2. In the (1.1–1.3) GeV $M(n\pi^+)$ effective mass interval the distributions predicted by the DRY model tend to increase with increasing pomeron slope. The peaks in the forward direction increase with increasing pomeron slope in (1.3–1.5) GeV $M(n\pi^+)$ effective mass interval but in the backward direction they decrease with increasing pomeron slope. For the effective $M(n\pi^+)$ mass from (1.5–1.7) GeV all the curves are peaked in the forward direction. In the PS model this is independent of the kinematical cuts but in the DRY model (and apparently in the experimental data) the role of kinematical cuts is crucial.

Its is seen that the best curves are obtained from the DRY model with pomeron slope of 0.5. Independently of the kinematical cuts the predictions of these models in the very forward direction do not agree with the data as in spite of kinematical cuts the data do not show pronounced dips at $\cos \Theta_{GJ} \sim 1$.

3f. Distribution in the Treiman-Yang angle $\Phi_{TY}(n\pi^+)$

The Treiman-Yang angle $\Phi_{TY}(n\pi^+)$ is defined in Eq. (A2.2). Its distribution between the neutron and the π meson is shown in Fig. 8 for invariant masses between (1.1–2.5 GeV). The experimental histogram exhibits a considerable anisotropy which proves that the t-channel helicity is not conserved in this process

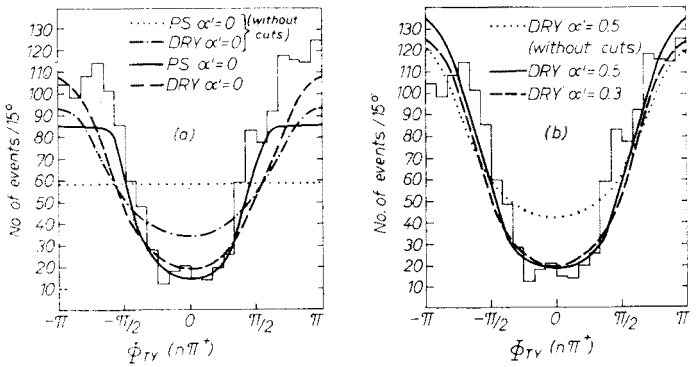

Fig. 8. Distribution of the Treiman-Yang angle $\Phi_{TY}(n\pi^+)$ in the $n\pi^+$ system for $1.1 < M(n\pi^+) < 2.5$ GeV; a) solid and dotted curves are the predictions of the PS model with and without kinematical cuts, dashed (dashed-dotted) curve corresponds to the DRY model for flat pomeron with (without) kinematical cuts; b) solid (dashed) curve corresponds to the DRY model predictions with 0.5 (0.3) pomeron slope, dotted curve is the prediction of DRY model for 0.5 pomeron slope without kinematical cuts

[21–22]. The DRY model predictions show an agreement with the data and this agreement improves with increasing pomeron slope. Without a kinematical cut in s_{3B} the PS model gives a completely flat distribution, which corresponds to t-channel helicity conservation. The cut lowers the curve around $\Phi = 0$ but there is still disagreement with the data around $\Phi = \pm\pi$.

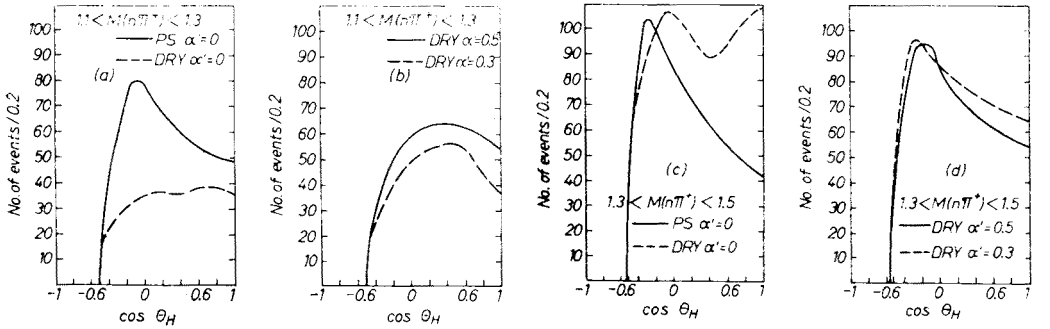

Fig. 9. Distribution in the $\cos \Theta_H(n\pi^+)$ of the $n\pi^+$ system in the $n\pi^+$ helicity frame; a) solid (dashed) curve corresponds to the PS (DRY) model for a flat pomeron for $1.1 < M(n\pi^+) < 1.3$ GeV; b) solid (dashed) curve corresponds to the DRY model predictions with 0.5 (0.3) pomeron slope for $1.1 < M(n\pi^+) < 1.3$ GeV; c) solid (dashed) curve corresponds to the PS (DRY) model for a flat pomeron for $1.3 < M(n\pi^+) < 1.5$ GeV; d) solid (dashed) curve corresponds to the DRY model predictions with 0.5 (0.3) pomeron slope for $1.3 < M(n\pi^+) < 1.5$ GeV

3g. Distribution in helicity angle $\cos \Theta_H(n\pi^+)$

The distribution in helicity angle $\cos \Theta_H$ is given in Figs 9 and 10. The helicity angle Θ_H is defined in A2.3). Unfortunately we have no data to check these predictions.

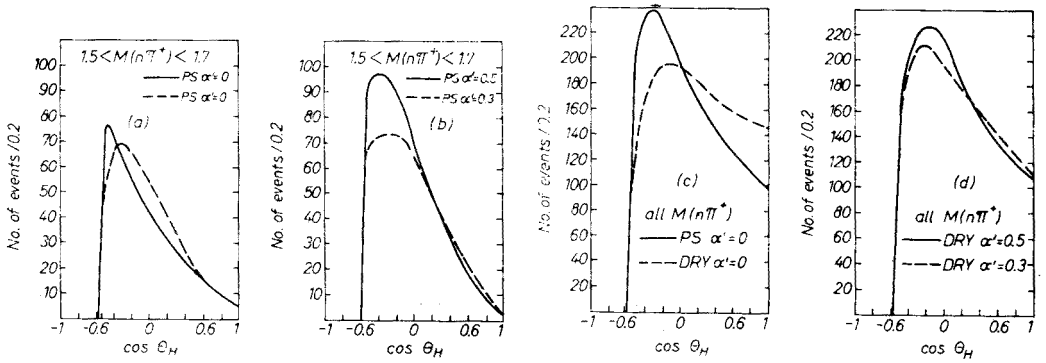

Fig. 10. Distribution in the $\cos \Theta_H(n\pi^+)$ of the $n\pi^+$ system in the $n\pi^+$ helicity frame: a) solid (dashed) curve corresponds to the PS (DRY) model for a flat pomeron for $1.5 < M(n\pi^+) < 1.7$ GeV; b) solid (dashed) curve corresponds to the DRY model predictions with 0.5 (0.3) pomeron slope for $1.5 < M(n\pi^+) < 1.7$ GeV; c) solid (dashed) curve corresponds to the PS (DRY) model for a flat pomeron for $1.1 < M(n\pi^+) < 1.7$ GeV; d) solid (dashed) curve corresponds to the DRY model predictions with 0.5 (0.3) pomeron slope for $1.1 < M(n\pi^+) < 1.7$ GeV

We see that all distributions are cut at $\cos \Theta_H \sim -0.6$. This is caused by the kinematical cut in s_{3B}. The PS model predicts in all $M(n\pi^+)$ effective mass intervals nearly the same shape, sharply peaked in the backward direction at $\cos \Theta_H \sim -0.6$. In the DRY model this peaking is flattened out at the lowest effective mass interval. With increasing pomeron slope in the forward direction the values of distributions decrease.

3h. Distribution in $\Phi_H(n\pi^+)$

The predicted angular distributions in the azimuthal angle $\Phi_H(n\pi^+)$ of the $n\pi^+$ system in the helicity frame (see (A2.4)) are presented in Fig. 11 for the $M(n\pi^+)$ effective mass from 1.1–1.7 GeV. All curves show an anisotropy in $\Phi_H(n\pi^+)$ which means that both models predict helicity non-conservation in the t-channel, too.

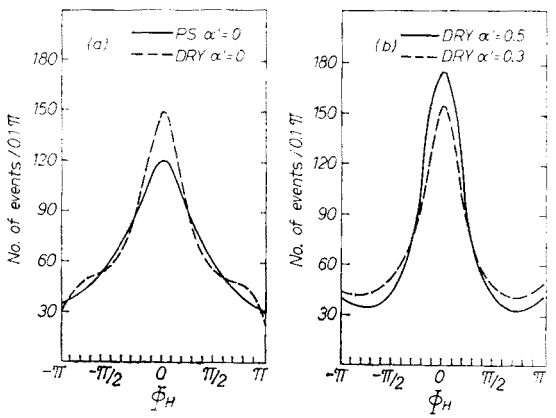

Fig. 11. Distribution of the azimuthal angle $\Phi_H(n\pi^+)$ in the helicity frame for $1.1 < M(n\pi^+) < 1.7$ GeV; a) solid (dashed) curve corresponds to the PS (DRY) model for a flat pomeron; b) solid (dashed) curve corresponds to the DRY model predictions with 0.5 (0.3) pomeron slope

We do not possess any data to check the predictions. The unpublished Scandinavian data at 19 GeV/c [20] show about the same shape as that predicted by both models. All curves are sharply peaked at $\Phi_H = 0$. In the DRY model this peaking increases with increasing pomeron slopes.

3i. The Chew-Low plot $\frac{d^2\sigma}{dMdt_1}$

In the diffractive process pp → pn π^+ the distribution on the Chew-Low plot may be fitted with the formula

$$\frac{d^2\sigma}{dMdt_1} = f(M)e^{b(M)t_1}, \tag{3.7}$$

where the slope $b(M)$ decreases from 20 GeV^{-2} to 5 GeV^{-2} in the Roper region of $M(n\pi^+)$. The PS model gives a linear dependence of log $d^2\sigma/dMdt_1$ on t_1 when $M(n\pi^+)$ is fixed. This holds for both trajectories

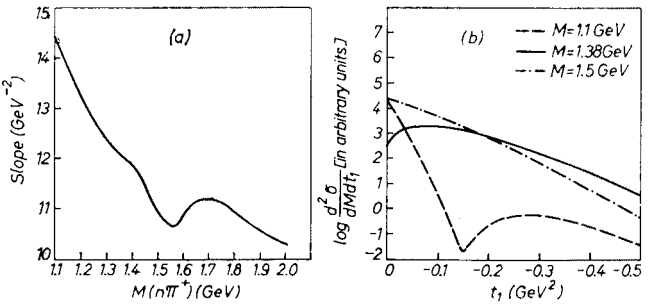

Fig. 12. a) slope $b(M)$ dependence on $M(n\pi^+)$ for the PS model; b) log $d^2\sigma/dMdt_1$ dependence on momentum-transfer-squared t_1 at three fixed values of $M(n\pi^+)$ for the N_α amplitude in the DRY model

N_α and N_γ. Fig. 12a shows the M-dependence of $b(M)$. However, only the N_γ trajectory in DRY model gives the same linear dependence of log $d^2\sigma/dMdt_1$ on t_1 at fixed $M(n\pi^+)$ values, while the N_α trajectory gives a linear behaviour at higher $|t_1|$ values for all pomeron slopes and all effective masses M. At low effective masses M ($1.08 < M < 1.3$ GeV) there is a dip at small $|t_1|$ values (*cf.* Fig. 12) which disappears at $M(n\pi^+) = 1.3$ GeV. Again there is a dip at $M(n\pi^+) = 1.38$ GeV and at small $|t_1|$, which vanishes with the increase of $M(n\pi^+)$. At $M(n\pi^+) = 1.38$ GeV the N_α amplitude has a pole (corresponding to the first daughter). In this case the dependence is not exponential and

$$\int d\Phi \int d\cos\Theta |M|^2 \sim e^{b(M)t_1} g(t_1), \tag{3.8}$$

where the polynomial $g(t_1)$ has a root at $t_1 \approx 0$, which is outside of the physical region. The curves in Fig. 12b show a characteristic behaviour of $d^2\sigma/dMdt_1|_{N_\alpha}$ for various values of $M(n\pi^+)$.

4. *Conclusions*

In this analysis, the Pokorski-Satz [4] and the Dorren-Rittenberg-Yaffe [6] models were tested for the process pp → pn π^+ at 12 GeV/c. In both models two parameters were varied: the overall normalization constant c, and the relative coupling constant λ of the baryon trajectories N_α and N_γ. The gross features of most of the distributions predicted by the two models are better described by the Dorren-Rittenberg-Yaffe model with non-zero pomeron slope than by the Pokorski-Satz model. Our conclusions can be summarized as follows:

A) The $M(n\pi^+)$ effective mass distribution, although reproduced in gross features, is not described in detail neither by the PS model nor by the DRY model. Both models give dips in the Roper region which are not observed in the experimental histogram.

B) The $M(p\pi^+)$ effective mass distribution given by the DRY model with higher pomeron slopes agrees with the data quite well, while in the PS model, being given only by the phase-space, the distribution does not reproduce the data.

C) The distribution in momentum transfer t_1 between the target proton and recoil proton is reproduced by both models only in gross features. However, the slope parameter which determines this distribution was not fitted in this analysis.

D) The momentum transfer t_2 distribution between the beam proton and the neutron is well described by the DRY model with pomeron slope higher than 0.3. The PS model gives too small values at higher $|t_2|$.

E) The angular distribution in the Gottfried-Jackson angle $\cos\Theta_{GJ}(n\pi^+)$ can be considered as a sensitive test of both models. In the higher $M(n\pi^+)$ effective mass values the PS model predicts only the enhancement in the forward direction independently of the kinematical cuts. This is contradicted by the data *e.g.* in the (1.3–1.5) GeV $M(n\pi^+)$ effective mass region. The DRY model predictions are the best for the pomeron slope of 0.5.

F) In the PS model the angular distribution in the Treiman-Yang angle $\Phi_{TY}(n\pi^+)$ is determined only by phase-space and is flat without the cut in s_{3B}. This means that helicity in t-channel is conserved in this model. The DRY model gives a non-flat distribution in $\Phi_{TY}(n\pi^+)$ even without the cut in s_{3B}. Therefore helicity in t-channel is not conserved in this model.

G) The distribution in the azimuthal angle $\Phi_H(n\pi^+)$ in the helicity frame shows an anisotropy in the two models (even without kinematical cuts), which means that the s-channel helicity is not conserved in both models.

H) The PS model predicts a decrease of the slope parameter $b(M)$ with increasing $M(n\pi^+)$ effective mass. However, this decrease is too small in the region of small values of effective mass. The explanation of this effect by the peripherality in the momentum transfer between the beam proton and the neutron is not correct [25].

There remain some problems to be explained. Firstly, the inclusion of spins of all the particles taking part in the interaction. This seems to be a difficult problem in the dual multiparticle amplitudes. Secondly, the inclusion of the empirical Gribov-Morrison rule $\Delta P = (-1)^{\Delta J}$ [24] which is not respected in neither model because the exchanged baryon Regge trajectories appear as parity doublets. Finally, it seems that the $M(n\pi^+)$ effective mass enhancement in the Roper region still remains to be explained. In this analysis we could not reproduce in detail the $M(n\pi^+)$ effective mass using the known resonances on the N_α and N_γ trajectories and the kinematical Deck effect in the framework of the dual models. The resonances were too narrow to describe the low $M(n\pi^+)$ effective mass enhancement in (1.2–1.65) GeV region.

The dynamical effect of the dip in the $d^2\sigma/dMdt_1$ distribution at small $|t_1|$ values predicted by the Dorren-Rittenberg-Yaffe model is not confirmed by the present data.

We would like to thank Professor A. Białas and Dr A. Kotański for stimulating discussions and for helpful criticism. We would also like to thank T. Jaroszewicz for useful discussions.

APPENDIX 1

Double Regge limit of DRY amplitude

We show here that the double Regge limit of the single Regge limit if the B_5 function is identical with the double Regge limit of the same B_5 function.

The single Regge limit of the B_5 function [9–11] is obtained by letting $s_{1A}, s_{3B} \to \infty$ at fixed $K = \alpha_{3B}/\alpha_{1A}$. As in the double Regge limit $s_{23} \to \infty$ with $\xi = -K\alpha_{23}$ fixed and K must then tend to 0. Substituting $x = \exp(z/\alpha_{23})$ in the first and the third integrals in Eqs (2.3), expanding all exponentials containing K up to the terms of the order $O(\alpha_{23}^{-1})$ and putting $K = \xi/\alpha_{23}$, the integrals become

$$(-\alpha_{23})^{-\alpha_{12}} \int_0^\infty dz\, e^{-z} z^{-\alpha_{12}-1} \left(-\frac{z}{\alpha_{23}} - \frac{\xi}{\alpha_{23}}\right)^{\alpha_p} \tag{A1.1a}$$

and

$$(-\alpha_{13})^{-\beta_{12}} \int_0^\infty dz\, e^{-z} z^{-\alpha_{12}-1} \left(\frac{z}{\alpha_{13}} + \frac{\xi}{\alpha_{13}}\right)^{\alpha_p} \tag{A1.1b}$$

respectively. The second integral in Eq. (2.3) vanishes due to the increasing imaginary part of α_{23} when $s_{23} \to \infty$. Had we neglected K in Eq. (2.3) we should also have neglected the terms ξ/α_{23} and ξ/α_{13} in both integrals (A1.1). Doing that we would receive the same result as in Ref. [6].

Making another substitution $z = \xi u$ and noting that $\alpha_{13} \approx -\alpha_{23}$ when $s_{23} \to \infty$, the sum of both integrals (A1.1) is equal to

$$(-1)^{\alpha_p}(1+e^{-i\pi\alpha_{12}})\Gamma(-\alpha_{12})\left(\frac{\alpha_{23}}{\xi}\right)^{\alpha_{12}-\alpha_p} \Psi(-\alpha_{12}, 1-\alpha_{12}+\alpha_p; \xi), \tag{A1.2}$$

where

$$\Psi(-\alpha_{12}, 1-\alpha_{12}+\alpha_p; \xi) = \frac{\xi^{\alpha_{12}}}{\Gamma(-\alpha_p)\Gamma(-\alpha_{12})} \iint_0^\infty dxdy x^{-\alpha_p-1} y^{-\alpha_{12}-1} e^{-x-y-xy/\xi}. \tag{A1.3}$$

Then using Eqs (A1.2) and (A1.3), the double Regge limit of (2.3) is finally obtained

$$-\alpha_p\beta(t_1)(1+e^{-i\pi\alpha_p})(1+e^{-i\pi\alpha_{12}})(\alpha_{23})^{\alpha_{12}}(\alpha_{3B})^{\alpha_p} \iint_0^\infty dxdy x^{-\alpha_p-1} y^{-\alpha_{12}-1} e^{-x-y-xy/\xi}. \tag{A1.4}$$

This is the same expression as for the double Regge limit of the B_5 function, apart from the factor $-\alpha_p\beta(t_1)$ which was introduced phenomenologically into Eq. (2.3) in Ref. [6].

APPENDIX 2

Definition of polar and azimuthal angles in Gottfried-Jackson and helicity frames

The Treiman-Yang angle $\Phi_{TY}(23)$ and the Gottfried-Jackson angle $\Theta_{GJ}(23)$ are defined as follows

$$\cos\Theta_{GJ}(23) = \left\{\frac{\vec{p}_1 \cdot \vec{p}_2}{|\vec{p}_1||\vec{p}_2|}\right\}_{\vec{p}_2+\vec{p}_3=0}, \tag{A2.1}$$

and

$$\cos\Phi_{TY}(23) = \left\{\frac{\vec{p}_B \times \vec{p}_1}{|\vec{p}_B \times \vec{p}_1|} \cdot \frac{\vec{p}_1 \times \vec{p}_2}{|\vec{p}_1 \times \vec{p}_2|}\right\}_{\vec{p}_2+\vec{p}_3=0} \tag{A2.2}$$

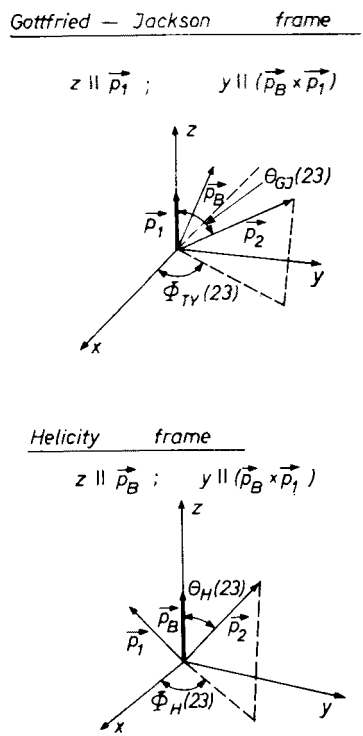

Fig. 13. Gottfried-Jackson and helicity frames for the $n\pi^+$ system

In the helicity frame we have the polar angle

$$\cos \Theta_{\mathrm{H}}(23) = \left\{ \frac{\vec{p}_B \cdot \vec{p}_2}{|\vec{p}_B|\,|\vec{p}_2|} \right\}_{\vec{p}_2+\vec{p}_3=0}, \tag{A2.3}$$

and the azimuthal angle

$$\cos \Phi_{\mathrm{H}}(23) = \left\{ \frac{\vec{p}_B \times \vec{p}_2}{|\vec{p}_B \times \vec{p}_2|} \cdot \frac{\vec{p}_B \times \vec{p}_1}{|\vec{p}_B \times \vec{p}_1|} \right\}_{\vec{p}_2+\vec{p}_3=0} \tag{A2.4}$$

All these formulae are written in the rest system of the 2 and 3 particles. The angles are illustrated in Fig. 13.

REFERENCES

[1] G. Veneziano, *Nuovo Cimento*, **57A**, 190 (1968).
[2] B. Petersson, N. A. Törnqvist, *Nucl. Phys.*, **B13**, 629 (1969).
[3] Chan Hong-Mo, R. O. Ratio, G. H. Thomas, N. A. Törnqvist, *Nuc. Phys.*, **B19**, 173 (1970).
[4] S. Pokorski, H. Satz, *Nucl. Phys.*, **B19**, 114 (1970).
[5] H. Satz, S. Schilling, *Nuovo Cimento*, **67A**, 511 (1970).
[6] J. D. Dorren, V. Rittenberg, D. Yaffe, *Nucl. Phys.*, **B30**, 306 (1971).
[7] J. Bartsch *et al.*, *CERN preprint* D. Ph. 1148 (1970).
[8] K. Paler *et al.*, *Nucl. Phys.*, **B33**, 13 (1971).
[9] K. Bardakçi, H. Ruegg, *Phys. Lett.*, **28B**, 342 (1968); M. A. Virasoro, *Phys. Rev. Lett.*, **22**, 37 (1969).

[10] A. Białas, S. Pokorski, *Nucl. Phys.*, **B10**, 339 (1969).
[11] B. E. Y. Svensson, *Elementary Review of the Veneziano Model Generalized to Multi-Particle Reaction*, University of Lund preprint, July 1970.
[12] M. Ross, Y. Y. Yam, *Phys. Rev. Lett.*, **19**, 546 (1967).
[13] A. Białas, W. Czyż, A. Kotański, *Nucl. Phys.*, **B46**, 109 (1972).
[14] L. Stodolsky, *Phys. Rev. Lett.*, **18**, 973 (1967).
[15] A. Białas, A. Kotański, private communication.
[16] I. S. Gradstein, I. M. Ryzhik, *Tables of Integrals, series and products*, Academic Press 1965.
[17] G. Yekutieli *et al.*, *Nucl. Phys.*, **B40**, 77 (1972).
[18] Bonn-Hamburg-München Collaboration, Max-Planck-Institut für Physik und Astrophysik München, preprint MPI-PAE/Exp. E1, 23, 1972.
[19] F. James, CERN library program W505.
[20] H. I. Miettinen, *A Phenomenological Analysis of the Reaction* $pp \to pn\pi^+$ *at Incoming Momenta between 4 and 30 GeV/c*, September 1971, Thesis, University of Helsinki.
[21] G. Cohen-Tannoudji *et al.*, *Phys. Lett.*, **33B**, 183 (1970).
[22] A. Białas, J. Dąbkowski, L. Van Hove, *Nucl. Phys.*, **B27**, 338 (1971).
[23] H. Satz, K. Schilling, *Aspects of Diffraction Dissociation*, Proceedings of the Colloquium on Multiparticle Dynamics, Helsinki 1971, p. 185.
[24] D. R. O. Morrison, *Rapporteur's Talk given at the XV International Conference on High Energy Physics*, Kiev 1970.
[25] H. I. Miettinen, P. Pirilä, *Phys. Lett.*, **40B**, 127 (1972).